

Detecting quantum critical points at finite temperature via quantum teleportation

G. A. P. Ribeiro and Gustavo Rigolin*

Departamento de Física, Universidade Federal de São Carlos, 13565-905, São Carlos, SP, Brazil

(Dated: April 6, 2023)

We show that the quantum teleportation protocol is a powerful tool to study quantum phase transitions (QPTs) at finite temperatures. We consider a pair of spins from an infinite spin-1/2 chain (XXZ model) in equilibrium with a reservoir at temperature T as the resource used by Alice and Bob to implement the teleportation protocol. We show that the efficiency of this pair of spins to teleport a qubit is drastically affected after we cross a quantum critical point (QCP), even for high values of T . Also, we show that the present tool is as sharp as quantum discord (QD) to spotlight a QCP, where QD is the best finite T QCP detector known to date. Contrary to QD, however, we show that the present tool is easier to compute theoretically and has a direct experimental and operational meaning.

I. INTRODUCTION

A QPT is the abrupt change in the physical properties of a many-body system that occurs at the absolute zero temperature ($T = 0$) while we change its Hamiltonian H [1]. At $T = 0$ the system is completely described by its ground state, a function of H . If we slowly modify H we may reach a QCP in the parameter space where the macroscopic properties of the system abruptly change. This “change of phase” is driven solely by quantum fluctuations and is almost always characterized by a fundamental symmetry change in the system’s ground state and the emergence of an order parameter. For a magnetic system, for instance, the order parameter is the net magnetization which becomes non-null after the system enters the ferromagnetic phase.

The physical principle behind the quantum fluctuations is the Heisenberg uncertainty principle. There is no role for thermal fluctuations in a QPT since we are in principle at $T = 0$ and to drive the system from one phase to another we usually change a single quantity (tuning parameter) of H . Examples of tuning parameters are the coupling constants or external fields acting on the system. The superfluid-Mott insulator transition [2], the superconductor-insulator transition [3], and the ferromagnetic-paramagnetic transition in some metals [4] are paradigmatic examples of QPTs.

Many useful theoretical tools to investigate QPTs assume that we are exactly at $T = 0$. For a spin chain the QCPs are obtained by studying the behavior of its magnetization, bipartite [5] and multipartite [6] entanglement, and more general quantum correlations [7, 8] as functions of the tuning parameter. The extremal values of these quantities or discontinuities in their first and second order derivatives are important indicators of a QPT. However, from the experimental point of view, the $T = 0$ condition is unattainable due to the third law of thermodynamics and any small deviation from $T = 0$ brings to the table thermal fluctuations that excite the system

beyond the ground state, limiting severely our ability to properly detect a genuine QCP. A remarkable example of this limitation is the inability of the entanglement of formation (EoF) [9] and the magnetic susceptibility to detect a QPT in spin chains for $T > 0$. For very small values of T , the former is already zero before and after the QCPs and the latter is a smooth function of the tuning parameter with no indication of QPTs when we cross the QCPs [10, 11].

In Ref. [11], however, we showed that in the thermodynamic limit (infinite chains) thermal quantum discord (TQD) [12] is a key theoretical tool that bridges the gap between the $T = 0$ predictions of QPTs and the finite T experiments. For several classes of spin chains, we showed that TQD detects QCPs for relatively high values of T while at this same T EoF is already zero and other thermodynamic quantities, including the magnetic susceptibility, are not able to correctly point the QCP or are less efficient than TQD to properly identify it.

Notwithstanding its tremendous success to detect a QCP at finite T [11], the QD [13, 14] has two handicaps. First, the optimization problem that one needs to solve to obtain the QD is NP-complete [15]. This means that the computation of QD is an intractable problem as we increase the size of the Hilbert space of the system under investigation. It is thus very difficult to extend the analysis of spin-1/2 chains to higher spin chains [16]. Second, QD does not have an operational meaning. There is no direct experimental procedure whose outcome is the QD. We need first to obtain the system’s density matrix and then use it to compute the QD.

In this manuscript we present a tool that possesses all the outstanding features of TQD in detecting QCPs at finite T and, on top of that, does not have its two aforementioned handicaps. The present tool is based on the quantum teleportation protocol [17], where a pair of qubits in a spin chain are employed as the quantum resource needed to implement the quantum teleportation protocol [18, 19]. In Ref. [19], for two-spin systems in equilibrium with a thermal reservoir at temperature T , it was shown that the fidelity of the teleported state changes abruptly when we cross a QCP. Here we extend the results of Ref. [19] to more general settings, to more

*Electronic address: rigolin@ufscar.br

QCPs, and most importantly, we work in the thermodynamic limit.

II. THE XXZ MODEL

The spin-1/2 chain we study here in the thermodynamic limit ($L \rightarrow \infty$) is given by the following Hamiltonian ($\hbar = 1$),

$$H = \sum_{j=1}^L (\sigma_j^x \sigma_{j+1}^x + \sigma_j^y \sigma_{j+1}^y + \Delta \sigma_j^z \sigma_{j+1}^z). \quad (1)$$

We employ periodic boundary conditions and $\sigma_j^z, \sigma_j^y, \sigma_j^x$ are the standard Pauli matrices associated with the qubit j . The anisotropy Δ is our tuning parameter and at $T = 0$ this model has two QCPs [20]. At $\Delta = -1$ we have a first-order transition. The ground state changes from a ferromagnetic phase ($\Delta < -1$) to the critical antiferromagnetic one ($-1 < \Delta < 1$). At $\Delta = 1$ we have a continuous phase transition with the system becoming an Ising-like antiferromagnet when $\Delta > 1$.

In thermal equilibrium with a reservoir at temperature T , the density matrix describing this chain is $\rho = e^{-H/kT}/Z$, with $Z = \text{Tr}[e^{-H/kT}]$ the partition function and k Boltzmann's constant. Tracing out from ρ all but two nearest neighbors gives the two-spin state [11]

$$\rho_{j,j+1} = \begin{pmatrix} \frac{1 + \langle \sigma_j^z \sigma_{j+1}^z \rangle}{4} & 0 & 0 & 0 \\ 0 & \frac{1 - \langle \sigma_j^z \sigma_{j+1}^z \rangle}{4} & \frac{\langle \sigma_j^x \sigma_{j+1}^x \rangle}{2} & 0 \\ 0 & \frac{\langle \sigma_j^x \sigma_{j+1}^x \rangle}{2} & \frac{1 - \langle \sigma_j^z \sigma_{j+1}^z \rangle}{4} & 0 \\ 0 & 0 & 0 & \frac{1 + \langle \sigma_j^z \sigma_{j+1}^z \rangle}{4} \end{pmatrix}. \quad (2)$$

The computation of the two-point correlation functions $\langle \sigma_j^\alpha \sigma_{j+1}^\alpha \rangle = \text{Tr}[\sigma_j^\alpha \sigma_{j+1}^\alpha \rho]$, with $\alpha = x, z$, in the thermodynamic limit for arbitrary T and Δ was done in Refs. [21–24] and reviewed in Ref. [11] (see Appendix A).

III. THE TELEPORTATION PROTOCOL

Equation (2) describes the resource through which we implement the teleportation protocol. Setting $j = 2$, the two-qubit state at sites 2 and 3 (see Fig. 1) is what one usually calls the state shared by Alice and Bob at the beginning of the teleportation protocol. The qubit to be teleported (spin 1 in Fig. 1) is external to the chain and can be prepared in any normalized pure state ($0 \leq r \leq 1$ and $0 \leq \gamma < 2\pi$),

$$|\psi\rangle = r|0\rangle + \sqrt{1-r^2}e^{i\gamma}|1\rangle. \quad (3)$$

The initial state describing the three qubits before the beginning of the teleportation protocol is

$$\rho = \rho_1 \otimes \rho_{23}, \quad (4)$$

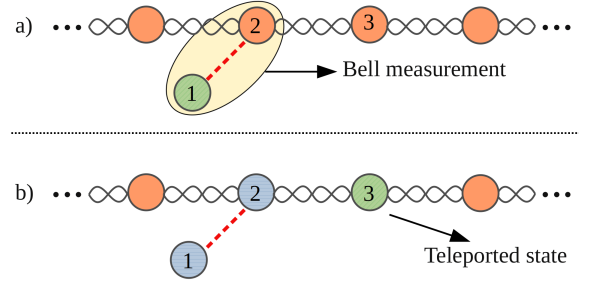


FIG. 1: (color online) The teleportation protocol works as follows [17]. Panel (a): First, one prepares the entangled resource (spins 2 and 3) to be used to teleport the input (spin 1). Second, a Bell measurement (BM) is made by Alice on spins 1 and 2. Panel (b): Third, Alice informs Bob of her BM result using a classical communication channel. Fourth, Bob applies a unitary operation on spin 3, which depends on Alice's BM result, to finish the protocol.

where $\rho_1 = |\psi\rangle\langle\psi|$ and ρ_{23} is given by Eq. (2). At the end of a given run of the protocol, i.e., after the four steps described in Fig. 1, Bob's qubit (spin 3) is given by [19]

$$\rho_{B_j} = \{U_j \text{Tr}_{12}[P_j \rho P_j] U_j^\dagger\} / Q_j(|\psi\rangle), \quad (5)$$

where Tr_{12} is the partial trace on Alice's qubits (spins 1 and 2). In Eq. (5), j denotes the BM result obtained by Alice, namely, $j = \Psi^-, \Psi^+, \Phi^-, \Phi^+$, and P_j the four projectors describing her BMs, $P_{\Psi^\pm} = |\Psi^\pm\rangle\langle\Psi^\pm|$ and $P_{\Phi^\pm} = |\Phi^\pm\rangle\langle\Phi^\pm|$, where the Bell states are $|\Psi^\mp\rangle = (|01\rangle \mp |10\rangle)/\sqrt{2}$ and $|\Phi^\mp\rangle = (|00\rangle \mp |11\rangle)/\sqrt{2}$.

Alice's probability to measure Bell state j is

$$Q_j(|\psi\rangle) = \text{Tr}[P_j \rho] \quad (6)$$

and the unitary operation that Bob must implement on his qubit after being informed of Alice's BM result is U_j .

The unitary operation U_j that Bob must implement on his qubit at the end of the protocol is also dependent on the entangled resource shared by Alice and Bob. In its standard formulation [17], where they share a maximally entangled pure state (Bell state), we have

$$S_{\Phi^+} = \{U_{\Phi^+}, U_{\Phi^-}, U_{\Psi^+}, U_{\Psi^-}\} = \{\mathbb{1}, \sigma^z, \sigma^x, \sigma^z \sigma^x\} \quad (7)$$

if the shared Bell state is $|\Phi^+\rangle$, with $\mathbb{1}$ being the identity matrix, and for $|\Phi^-\rangle$ and $|\Psi^\pm\rangle$, we have, respectively,

$$S_{\Phi^-} = \{U_{\Phi^+}, U_{\Phi^-}, U_{\Psi^+}, U_{\Psi^-}\} = \{\sigma^z, \mathbb{1}, \sigma^z \sigma^x, \sigma^x\}, \quad (8)$$

$$S_{\Psi^+} = \{U_{\Phi^+}, U_{\Phi^-}, U_{\Psi^+}, U_{\Psi^-}\} = \{\sigma^x, \sigma^z \sigma^x, \mathbb{1}, \sigma^z\}, \quad (9)$$

$$S_{\Psi^-} = \{U_{\Phi^+}, U_{\Phi^-}, U_{\Psi^+}, U_{\Psi^-}\} = \{\sigma^z \sigma^x, \sigma^x, \sigma^z, \mathbb{1}\}. \quad (10)$$

In the present case, the state ρ_{23} shared by Alice and Bob is not pure and is approximately described by one Bell state in one phase and by a different one in another phase. Therefore, when characterizing the QCPs of a spin chain we will work with the four possible sets of unitary operations above. As we will see, this approach

is crucial to obtain the most efficient QCP detector based on the teleportation protocol.

To quantify the similarity between the teleported state, Bob's qubit at the end of the protocol (spin 3), with the input state teleported by Alice (spin 1), we use the fidelity [25]. For a pure input state we have

$$F_j(|\psi\rangle, S_k) = \langle \psi | \rho_{B_j} | \psi \rangle, \quad (11)$$

where $|\psi\rangle$ is given by Eq. (4) and ρ_{B_j} by Eq. (5). If the teleported state is exactly the input state, $F_j = 1$, and $F_j = 0$ if the output is orthogonal to the input. Note that in general F_j depends on the input state, the entangled resource shared by Alice and Bob, and on the set of unitary corrections S_k chosen by Bob. Here the entangled resource is fixed and given by Eq. (2), while we can freely choose $|\psi\rangle$ and S_k , with $k = \Psi^\mp, \Phi^\mp$.

For a fixed input state, after several runs of the protocol the mean fidelity (efficiency) is [26, 27]

$$\overline{F}(|\psi\rangle, S_k) = \sum_{j=\Psi^\mp, \Phi^\mp} Q_j(|\psi\rangle) F_j(|\psi\rangle, S_k). \quad (12)$$

If we want an input state independent measure of the efficiency of the teleportation protocol, we can average over all states on the Bloch sphere. This is equivalent to considering in Eq. (3) r^2 and γ as independent continuous random variables over their allowed values [26, 27]. Formally, this input state independent mean fidelity, average fidelity for short, can be written as [19, 26–28]

$$\langle \overline{F}(S_k) \rangle = \int_{\Omega} \overline{F}(|\psi\rangle, S_k) \mathcal{P}(|\psi\rangle) d|\psi\rangle, \quad (13)$$

where we integrate over the sample space Ω comprising of all qubits on the Bloch sphere and $\mathcal{P}(|\psi\rangle)$ is the corresponding uniform probability distribution over Ω .

Before we specialize to the XXZ model, we should remark that, from an experimental point of view, the present analysis is meaningful when the time needed to execute the four steps of the teleportation protocol is shorter than the time needed by the system to get back to equilibrium with the thermal reservoir. The rate at which we implement all the four steps of the protocol should be greater than the thermal relaxation rate of the system. We should determine the state of the qubit teleported to Bob before it thermalizes once again. Nevertheless, the experimental procedure needed to teleport a qubit and measure Bob's state is clear and can in principle be implemented using state of the art techniques [29–35]. Knowing Bob's state at the end of the teleportation protocol for a representative sample of input states lying on the Bloch sphere is all we need to determine Eqs. (12) and (13). This should be contrasted to the determination of the EoF or the QD of a pair of spins. There is no direct experimental procedure to measure those quantities for arbitrary mixed states. To compute those quantities we must have access to the complete density matrix describing the two qubits (spins 2 and 3) [9, 13, 14]. For

the XXZ model, for instance, we must have the complete knowledge of Eq. (2). On the other hand, to experimentally determine Bob's state at the end of the teleportation protocol we just need the single qubit density matrix describing it. We only need to measure one-point correlation functions instead of the two-point ones needed to the computation of the EoF or the QD.

IV. RESULTS

If we insert Eq. (4) into (6) we get $Q_j(|\psi\rangle) = 1/4$, for all j . This means that Alice obtains with equal chances any one of the four Bell states after the BM on qubits 1 and 2. Note that the probabilities Q_j are all independent of the input state (qubit 1). This is a particular feature of the XXZ model without external fields and can be traced back to the specific form of Eq. (2).

Another feature of the present model is that Eq. (11) leads to $F_{\Psi^\mp}(|\psi\rangle, S_k) = F_{\Phi^\mp}(|\psi\rangle, S_k)$. In other words, F_j is independent of j , i.e., independent of the outcome of Alice's BM. Therefore, for the present model, Eq. (12) can be written as $\overline{F}(|\psi\rangle, S_k) = F_j(|\psi\rangle, S_k)$, any j .

If we maximize over all pure states and over S_k we get for the overall maximum fidelity (see Appendix B),

$$\overline{\mathcal{F}} = \max_{\{|\psi\rangle, S_k\}} \overline{F}(|\psi\rangle, S_k) = \max \left[\frac{1 + |\langle \sigma_2^z \sigma_3^z \rangle|}{2}, \frac{1 + |\langle \sigma_2^x \sigma_3^x \rangle|}{2} \right]. \quad (14)$$

The extrema of Eq. (12) occur for the input states $|\psi\rangle = |1\rangle$ and $|\psi\rangle = (|0\rangle + e^{i\gamma}|1\rangle)/\sqrt{2}$ (see Appendix B). Which state leads to the maximum (or minimum) fidelity depends on the phase of the spin chain and on the sign of the two-point correlation functions.

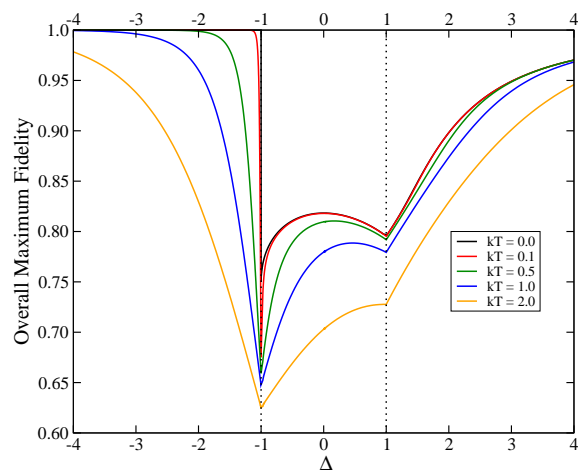


FIG. 2: (color online) $\overline{\mathcal{F}}$, Eq. (14), as a function of the anisotropy Δ that characterizes the XXZ model [Eq. (1)]. Both QCPs are detected at $T = 0$ and $T > 0$ by a discontinuity in the first derivative of $\overline{\mathcal{F}}$ with respect to Δ . Here and in all other figures all quantities are dimensionless.

In Fig. 2 we plot $\overline{\mathcal{F}}$ as a function of Δ for several values of T . It is clear from Fig. 2 that $\overline{\mathcal{F}}$ detects both QCPs

when $T = 0$ and for $T > 0$. It is worth mentioning that for $kT \gtrsim 0.1$ the EoF is already zero before, at, and after the QCP $\Delta = -1$ [11]. The cusp-like behavior of $\overline{\mathcal{F}}$ at the two QCPs is similar to the one observed for the TQD [11]. The discontinuity of the first derivative of $\overline{\mathcal{F}}$ with respect to the tuning parameter Δ is related to the fact that at the two QCPs the roles of $|\langle \sigma_2^z \sigma_3^z \rangle|$ and $|\langle \sigma_2^x \sigma_3^x \rangle|$ are exchanged. For instance, in one phase the maximum of $\overline{\mathcal{F}}$ is a function of $|\langle \sigma_2^z \sigma_3^z \rangle|$ while at the other phase it is a function of $|\langle \sigma_2^x \sigma_3^x \rangle|$.

If we now employ Eq. (13), maximized over the sets S_k of unitary operations available to Bob, we get (see Appendix B)

$$\begin{aligned} \langle \overline{\mathcal{F}} \rangle &= \max_{\{S_k\}} \langle \overline{\mathcal{F}}(S_k) \rangle \\ &= \max \left[\frac{3+2|\langle \sigma_2^x \sigma_3^x \rangle| - \langle \sigma_2^z \sigma_3^z \rangle}{6}, \frac{3 + \langle \sigma_2^z \sigma_3^z \rangle}{6} \right]. \end{aligned} \quad (15)$$

Looking at Fig. 3 we realize that the QCP located at $\Delta = -1$, associated with a first order QPT, is clearly detected for $T = 0$ and $T > 0$. The cusp-like behavior of $\langle \overline{\mathcal{F}} \rangle$ at $\Delta = -1$ for $T = 0$ and $T > 0$ clearly indicates a QPT. The other QCP, $\Delta = 1$, related to a continuous QPT is detected at $T = 0$ by noting that $\langle \overline{\mathcal{F}} \rangle$ has its global maximum exactly at $\Delta = 1$. For finite T this maximum is displaced to higher values of Δ . Contrary to $\overline{\mathcal{F}}$, $\langle \overline{\mathcal{F}} \rangle$ does not have a cusp at $\Delta = 1$. However, if we work with both the maximum and minimum of $\langle \overline{\mathcal{F}}(S_k) \rangle$, we can get a cusp-like behavior at both QCPs (see Appendix C).

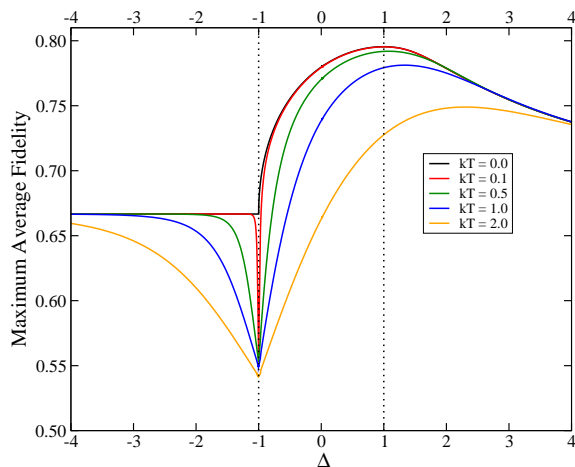


FIG. 3: (color online) Same as Fig. 2 but now we plot $\langle \overline{\mathcal{F}} \rangle$, Eq. (15). The QCP at $\Delta = -1$ is detected at $T = 0$ and $T > 0$ by a discontinuity in the first derivative of $\langle \overline{\mathcal{F}} \rangle$ with respect to Δ . The other QCP is obtained at $T = 0$ noting that $\langle \overline{\mathcal{F}} \rangle$ is maximal at $\Delta = 1$. For finite T , the maximum is displaced to greater values of Δ . For $kT \lesssim 1.0$ these maxima lie close together and by extrapolating to $kT \rightarrow 0$ we can infer this QCP by working with finite T data.

The usefulness of $\overline{\mathcal{F}}$ and $\langle \overline{\mathcal{F}} \rangle$ to pinpoint a QCP is not restricted to the XXZ model. They are as good as TQD

[11] to detect for $T > 0$ the QCP of the XXX model (see Appendix D). It remains an open problem to check if the ideas here presented apply to the detection of pseudo-transitions [36, 37].

V. DISCUSSION AND CONCLUSION

As already highlighted above, the operational and experimental interpretation of the fidelities is very clear and straightforward. For the XXZ and XXX model with no fields, whose two-qubit density matrix is given by Eq. (2), the experimental demands to implement the present proposal is further reduced. Since for those models $\overline{\mathcal{F}}(|\psi\rangle, S_k) = F_j(|\psi\rangle, S_k)$, we do not need to implement any unitary correction U_j on the teleported qubit to obtain the fidelities. We just need to separate the data into four sets, each one corresponding to the four possible outcomes of Alice's BMs. In this way, we automatically get the mean fidelities $\overline{\mathcal{F}}(|\psi\rangle, S_k)$ related to each one of the four sets S_k . Teleporting a representative sample of qubits covering the Bloch sphere, we obtain $\overline{\mathcal{F}}$ picking from this sample of teleported states the case yielding the greatest fidelity and, averaging over all cases, we get $\langle \overline{\mathcal{F}} \rangle$. To fully execute the teleportation protocol we also need to be able to implement the BMs on qubits 1 and 2. The BMs can be made by applying a controlled-not (CNOT) operation on those qubits [29–35] followed by a Hadamard operation on the control qubit and a measurement of those spins in the computational basis [38]. For instance, if after the previous prescription we see spins 1 and 2 pointing up ($|00\rangle$) or down ($|11\rangle$), it means that we have projected them onto the Bell state $|\Phi^+\rangle$ or $|\Psi^-\rangle$ [38].

From the theoretical point of view, and similarly to EoF and QD, we need the two-qubit density matrix, Eq. (2), to compute the fidelity. In a more general scenario (higher spins), we need the bipartite density matrix describing two N -dimensional systems. However, and contrary to EoF and QD, the computational resources needed to compute the fidelity are less demanding. To compute the maximum average fidelity, Eq. (15), we just need to repeat for each one of the four sets of unitary operations S_k the calculation of the average fidelity, Eq. (13). The calculation of the latter is a very simple matter and can be efficiently scaled to an N -dimensional input state $|\psi\rangle$ [27]. To calculate the overall maximum fidelity, Eq. (14), we have to repeat the maximization of Eq. (12) over all input states $|\psi\rangle$ four times (for each one of the four sets of unitary operations S_k). Since an N -dimensional pure state is describe by $2N - 2$ independent parameters [39], we will face an optimization problem involving $2N - 2$ free variables. For high values of N this is not a simple problem but it is less demanding than solving the corresponding optimization problem to determine the QD, where we must minimize the conditional entropy over all sets of generalized measurements (POVMs) [13–15]. These POVMs are $N \times N$ matrices and the number

of free parameters increases faster than linearly with N [15]. The intuitive reason for this difference in computational demand rests on the fact that for the overall maximum fidelity we optimize over a single pure state while for QD the optimization problem is equivalent to the complexity of determining the EoF, whose optimization is done over all ensembles of pure states into which ρ_{23} can be decomposed [15].

Summing up, we have presented two teleportation based theoretical tools to detect QCPs at finite T equivalent to TQD, the most reliable QCP detector for finite T known to date. Both tools work without the knowledge of the order parameter associated with the QPT. The tools here presented have two features that set them apart from TQD and other quantum information theory based QCP detectors. First, they have a straightforward experimental interpretation and can in principle be directly measured in the laboratory. Second, from a theoretical point of view we need less computational resources to calculate them when compared to TQD, with one of these tools, the average fidelity, easily scalable to an N -dimensional spin system.

Acknowledgments

GR thanks the Brazilian agency CNPq (National Council for Scientific and Technological Development) for funding and CNPq/FAPERJ (State of Rio de Janeiro Research Foundation) for financial support through the National Institute of Science and Technology for Quantum Information.

Appendix A: Two-point correlation functions

The XXZ model we studied is given by Eq. (1) of the main text. In thermal equilibrium with a reservoir at temperature T , the non-null two-point correlation functions are $\langle \sigma_j^x \sigma_{j+1}^x \rangle = \langle \sigma_j^y \sigma_{j+1}^y \rangle$ and $\langle \sigma_j^z \sigma_{j+1}^z \rangle$. The techniques to solve this problem in the thermodynamic limit (infinite chain) were developed in Refs. [21–24] and they were carefully reviewed, adapted, and implemented for the present context in Ref. [11].

At the absolute zero temperature, the two-point correlation functions are given by Figs. 4 and 5 [11].

For finite T , the behavior of the two-point correlation functions are given by Figs. 6 and 7 [11].

Note that at the quantum critical points (QCPs) the two-point correlation function having the greatest magnitude changes. This is particularly clear for low values of kT . Before $\Delta = -1$, $|\langle \sigma_j^z \sigma_{j+1}^z \rangle| > |\langle \sigma_j^x \sigma_{j+1}^x \rangle|$ while after $\Delta = -1$, $|\langle \sigma_j^x \sigma_{j+1}^x \rangle| > |\langle \sigma_j^z \sigma_{j+1}^z \rangle|$. This behavior is also seen before and after the other QCP at $\Delta = 1$ and it is the reason for the cusp like behavior of the overall maximum fidelity $\overline{\mathcal{F}}$ at both QCPs (see main text).

XXZ model ($kT = 0.0$)

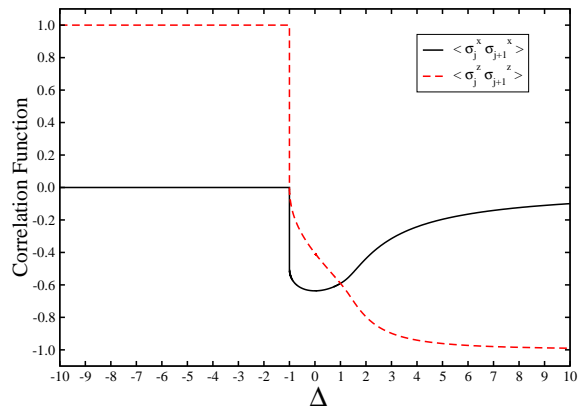


FIG. 4: (color online) Two-point correlation functions in the thermodynamic limit at $T = 0$ as a function of the tuning parameter Δ .

XXZ model ($kT = 0.0$)

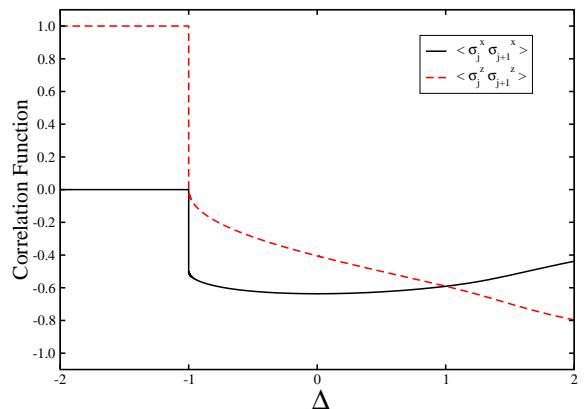


FIG. 5: (color online) Two-point correlation functions in the thermodynamic limit at $T = 0$ as a function of the tuning parameter Δ .

Appendix B: Obtaining $\overline{\mathcal{F}}$ and $\langle \overline{\mathcal{F}} \rangle$

In the XXZ model, we have $Q_j(|\psi\rangle) = 1/4$ and $F_j(|\psi\rangle, S_k) = F_{j'}(|\psi\rangle, S_k)$ for any $j, j' = \Psi^\mp, \Phi^\mp$. Thus, a direct calculation using Eqs. (3)-(5) and (11) of the main text allows us to write Eq. (12) of the main text as follows

$$\overline{F}(|\psi\rangle, S_{\Psi^-}) = f(r, -xx, zz), \quad (\text{B1})$$

$$\overline{F}(|\psi\rangle, S_{\Psi^+}) = f(r, xx, zz), \quad (\text{B2})$$

$$\overline{F}(|\psi\rangle, S_{\Phi^-}) = g(r, \gamma, -xx, zz), \quad (\text{B3})$$

$$\overline{F}(|\psi\rangle, S_{\Phi^+}) = g(r, \gamma, xx, zz), \quad (\text{B4})$$

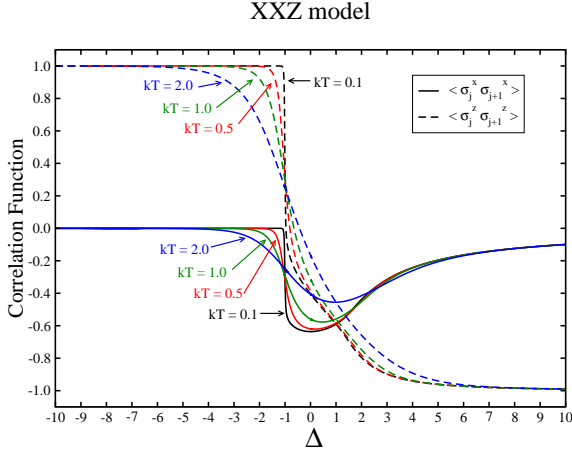


FIG. 6: (color online) Two-point correlation functions in the thermodynamic limit for $T > 0$ as a function of the tuning parameter Δ .

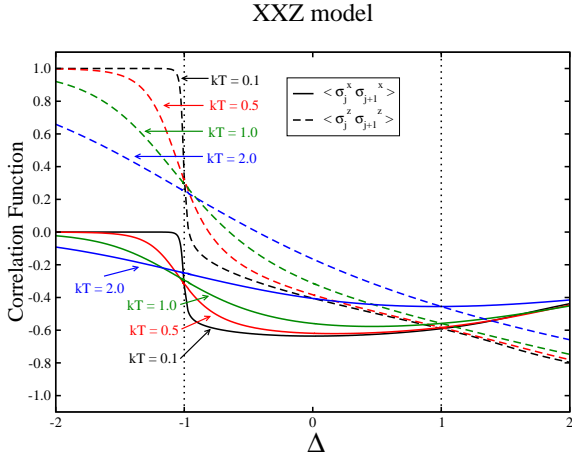


FIG. 7: (color online) Two-point correlation functions in the thermodynamic limit for $T > 0$ as a function of the tuning parameter Δ .

where

$$f(r, xx, zz) = [1 + 4r^2(1 - r^2)(xx + zz) - zz]/2 \quad (\text{B5})$$

$$g(r, \gamma, xx, zz) = [1 + (1 - 2r^2)^2 zz + 4r^2(1 - r^2)xx \cos(2\gamma)]/2, \quad (\text{B6})$$

$$xx = \langle \sigma_j^x \sigma_{j+1}^x \rangle, \quad (\text{B7})$$

$$zz = \langle \sigma_j^z \sigma_{j+1}^z \rangle. \quad (\text{B8})$$

Computing the extrema of $f(r, xx, zz)$, i.e., solving

$$\frac{\partial f}{\partial r} = 0, \quad (\text{B9})$$

we immediately get for $r \geq 0$

$$r = 0, 1/\sqrt{2}. \quad (\text{B10})$$

This means, according to Eq. (3) of the main text, that the states leading to the extrema of $\overline{F}(|\psi\rangle, S_{\Psi\mp})$ are, up to an overall phase, either $|1\rangle$ or $(|0\rangle + e^{i\gamma}|1\rangle)/\sqrt{2}$.

If we now compute the extrema of $g(r, \gamma, xx, zz)$, namely, if we solve

$$\frac{\partial g}{\partial r} = 0, \quad (\text{B11})$$

$$\frac{\partial g}{\partial \gamma} = 0, \quad (\text{B12})$$

we obtain

$$(r; \gamma) = (0; 0 \leq \gamma < 2\pi), \quad (\text{B13})$$

$$(r; \gamma) = (1/\sqrt{2}; 0, \pi/2, \pi, 3\pi/2). \quad (\text{B14})$$

This implies that the input states leading to the extrema of $\overline{F}(|\psi\rangle, S_{\Psi\mp})$ are, up to an overall phase, $|1\rangle$, $(|0\rangle \pm |1\rangle)/\sqrt{2}$, and $(|0\rangle \pm i|1\rangle)/\sqrt{2}$.

Inserting the corresponding values of r and γ for the extrema of the fidelity we get

$$\overline{F}(r = 0, S_{\Psi\mp}) = (1 - zz)/2, \quad (\text{B15})$$

$$\overline{F}(r = 1/\sqrt{2}, S_{\Psi\mp}) = (1 \mp xx)/2, \quad (\text{B16})$$

$$\overline{F}(r = 0, S_{\Phi\mp}) = (1 + zz)/2, \quad (\text{B17})$$

$$\overline{F}(r = 1/\sqrt{2}, \gamma, S_{\Phi\mp}) = [1 \mp xx \cos(2\gamma)]/2. \quad (\text{B18})$$

Therefore, Eqs. (B15)-(B18) lead to

$$\overline{\mathcal{F}} = \max_{\{|\psi\rangle, S_k\}} \overline{F}(|\psi\rangle, S_k) = \max \left[\frac{1 + |zz|}{2}, \frac{1 + |xx|}{2} \right], \quad (\text{B19})$$

which is exactly Eq. (14) of the main text.

Moving to the calculation of $\langle \overline{\mathcal{F}} \rangle$, we first note that if we write the input state as

$$|\psi\rangle = a|0\rangle + b|1\rangle, \quad (\text{B20})$$

where $|a|^2 + |b|^2 = 1$, Eq. (13) of the main text becomes

$$\langle \overline{F}(S_{\Psi\mp}) \rangle = [(\langle |a|^4 \rangle + \langle |b|^4 \rangle)(1 - zz) + 2\langle |ab|^2 \rangle(1 \mp 2xx + zz)]/2. \quad (\text{B21})$$

If $|a|^2$, the probability of finding the input in the state $|0\rangle$, and the relative phase between the complex numbers a and b are given by two independent continuous uniform distributions, we have [26, 27]

$$\langle |a|^4 \rangle = \langle |b|^4 \rangle = 1/3, \quad \langle |ab|^2 \rangle = 1/6. \quad (\text{B22})$$

Note that we will obtain the same averages if we use the Bloch sphere representation for the input state [38],

$$|\psi\rangle = \cos(\theta/2)|0\rangle + \sin(\theta/2)e^{i\varphi}|1\rangle, \quad (\text{B23})$$

and average over the whole Bloch sphere. In this case, using the notation of Eq. (13) of the main text, $d|\psi\rangle = dA = \sin\theta d\theta d\varphi$ is the element of area of a unit sphere written in spherical polar coordinates, $\mathcal{P}(|\psi\rangle) = 1/(4\pi)$, $0 \leq \theta \leq \pi$, and $0 \leq \varphi \leq 2\pi$.

Thus, using Eq. (B22) we get for Eq. (B21),

$$\langle \overline{F}(S_{\Psi\mp}) \rangle = (3 \mp 2xx - zz)/6. \quad (\text{B24})$$

In an analogous way we obtain

$$\langle \overline{F}(S_{\Phi\mp}) \rangle = (3 + zz)/6, \quad (\text{B25})$$

where to arrive at Eq. (B25) we also used that

$$\langle (a^*b)^2 \rangle = \langle (ab^*)^2 \rangle = 0, \quad (\text{B26})$$

with $a^*(b^*)$ denoting the complex conjugate of $a(b)$. Finally, looking at Eqs. (B24) and (B25) we get

$$\begin{aligned} \langle \overline{F} \rangle &= \max_{\{S_k\}} \langle \overline{F}(S_k) \rangle \\ &= \max \left[\frac{3 + 2|xx| - zz}{6}, \frac{3 + zz}{6} \right], \end{aligned} \quad (\text{B27})$$

which is Eq. (15) of the main text.

Appendix C: Looking deeper at \overline{F} and $\langle \overline{F} \rangle$

In order to better understand the behavior of the curves shown in Fig. 2 of the main text, we will study the behavior of the following quantity,

$$\overline{F}(S_k) = \max_{\{|\psi\rangle\}} \overline{F}(|\psi\rangle, S_k). \quad (\text{C1})$$

Equation (C1) is the mean fidelity, Eq. (12) of the main text, maximized over the input states only. We want to investigate the behavior of $\overline{F}(S_k)$ for each one of the four possible values of k ,

$$\overline{F}(S_{\Psi\mp}) = \max \left[\frac{1 - zz}{2}, \frac{1 \mp xx}{2} \right], \quad (\text{C2})$$

$$\overline{F}(S_{\Phi\mp}) = \max \left[\frac{1 + zz}{2}, \frac{1 + |xx|}{2} \right]. \quad (\text{C3})$$

Proceeding in this way we will be able to trace back which expression is responsible to the behavior of \overline{F} shown in Fig. 2 of the main text.

In Fig. 8 we show Eqs. (C2) and (C3) at $T = 0$ and in Fig. 9 at $T > 0$ as a function of the tuning parameter Δ .

Looking at both Figs. 8 and 9, we realize that before the first QCP, $\Delta = -1$, the overall maximum fidelity \overline{F} is given by $\overline{F}(S_{\Phi\mp})$. Between the two QCPs we have either $\overline{F}(S_{\Phi\mp})$ or $\overline{F}(S_{\Psi-})$ as the maximum fidelity. And after the second QCP, $\Delta = 1$, it is $\overline{F}(S_{\Psi\mp})$ that dominates. The change of which $\overline{F}(S_k)$ dominates at the QCPs is the reason for the cusp-like behavior of \overline{F} .

A similar analysis allows us to understand the behavior of the maximum average fidelity $\langle \overline{F} \rangle$ as shown in Fig. 3 of the main text. We now investigate $\langle \overline{F}(S_k) \rangle$, Eq. (13) of the main text, for each one of the four possible values of k ,

$$\langle \overline{F}(S_{\Psi\mp}) \rangle = (3 \mp 2xx - zz)/6, \quad (\text{C4})$$

$$\langle \overline{F}(S_{\Phi\mp}) \rangle = (3 + zz)/6. \quad (\text{C5})$$

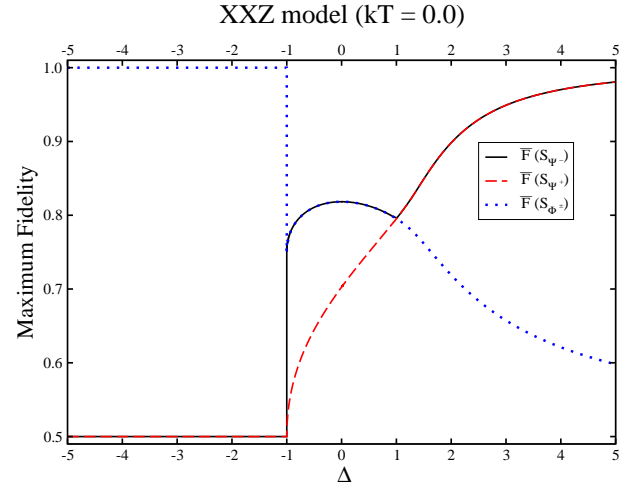


FIG. 8: (color online) $\overline{F}(S_k)$ as a function of Δ at the absolute zero temperature.

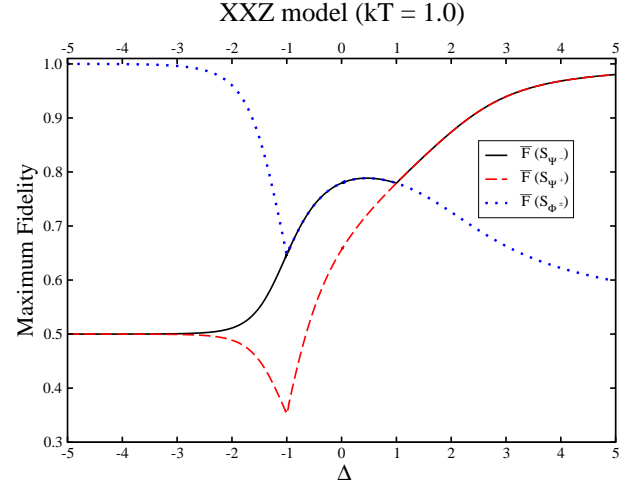


FIG. 9: (color online) Same as Fig. 8 but at $kT = 1.0$.

Looking at Figs. 10 and 11, we note that before the first QCP, $\Delta = -1$, the maximum average fidelity $\langle \overline{F} \rangle$ is given by $\langle \overline{F}(S_{\Phi\mp}) \rangle$. After the first QCP we have $\langle \overline{F}(S_{\Psi-}) \rangle$ as the maximum average fidelity. This trend continues even after the second QCP, where $\langle \overline{F}(S_{\Psi-}) \rangle$ achieves its maximum. That is why we do not see any cusp-like behavior at $\Delta = 1$, the second QCP. At this QCP, there is no change in the function maximizing the average fidelity. Before, at, and after $\Delta = 1$, it is always $\langle \overline{F}(S_{\Psi-}) \rangle$ that maximizes the average fidelity.

Incidentally, looking at Figs. 10 and 11, we realize that by monitoring both the maximum and the minimum average fidelity we can detect both QCPs via a cusp-like behavior. Indeed, monitoring the maximum average fidelity we see a cusp-like behavior at $\Delta = -1$, the first QCP. This is what is shown in Fig. 3 of the main text. However, if we plot the minimum average fidelity,

$$\langle \overline{F} \rangle_{min} = \min_{\{S_k\}} \langle \overline{F}(S_k) \rangle, \quad (\text{C6})$$

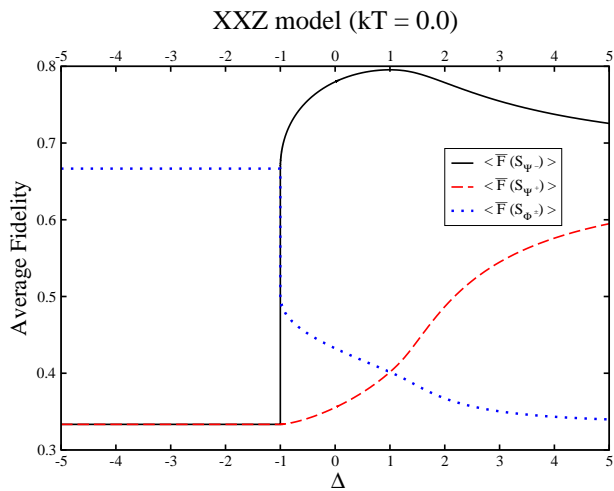


FIG. 10: (color online) $\langle \overline{F}(S_k) \rangle$ as a function of Δ at the absolute zero temperature.

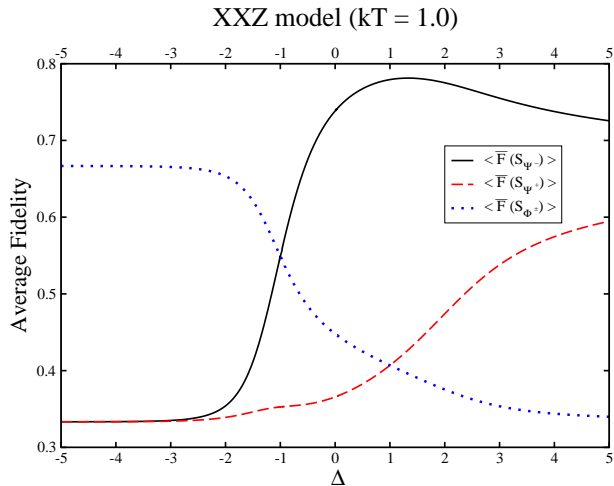


FIG. 11: (color online) Same as Fig. 10 but at $kT = 1.0$.

we will see a cusp-like behavior not in the first but in the second QCP. At $\Delta = 1$ we see that the function giving the minimum average fidelity changes. Before $\Delta = 1$ the minimum is achieved by $\langle \overline{F}(S_{\Psi^+}) \rangle$ and after it the minimum is given by $\langle \overline{F}(S_{\Phi^\mp}) \rangle$. This change of the function minimizing the average fidelity leads to a cusp-like behavior at this QCP. As such, by monitoring both the maximum and minimum of $\langle \overline{F}(S_k) \rangle$, we can build an input state independent fidelity as sharp as the state dependent fidelity in detecting both QCPs, with the advantage that the computation of the former quantity is easily scalable to high spin systems.

We finish this section showing $\overline{F}(S_{\Psi^-})$ and $\langle \overline{F}(S_{\Psi^-}) \rangle$ for several values of T . Although these quantities are not as good as $\overline{\mathcal{F}}$, $\langle \overline{\mathcal{F}} \rangle$, and $\langle \overline{\mathcal{F}} \rangle_{min}$ to pinpoint a QCP, we can obtain a lot of information about where the QCPs are located by working with them. We also obtain similar results working with $\overline{F}(S_k)$ and $\langle \overline{F}(S_k) \rangle$, where $k = \Psi^+, \Phi^\mp$.

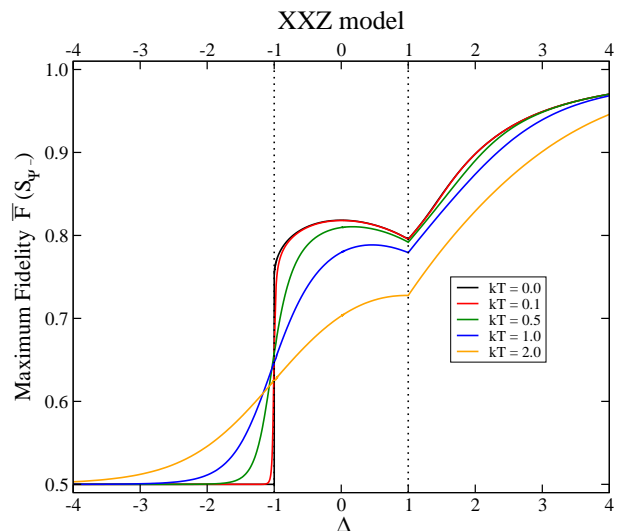


FIG. 12: (color online) $\overline{F}(S_{\Psi^-})$ as a function of Δ for several values of temperature. Temperatures increase from top to bottom when $\Delta > -1$.

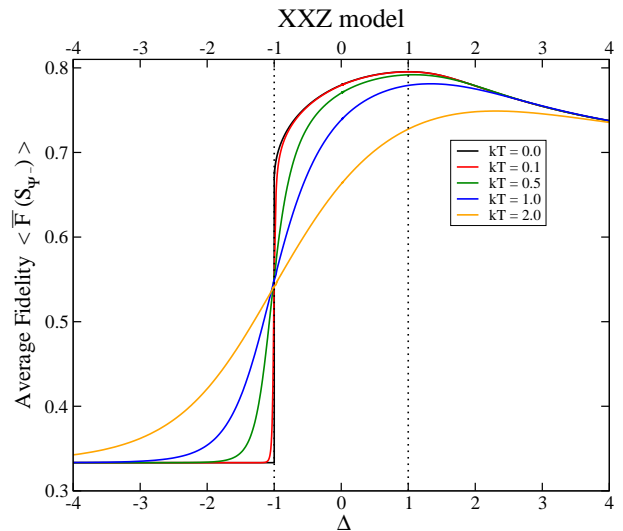


FIG. 13: (color online) $\langle \overline{F}(S_k) \rangle$ as a function of Δ for several values of temperature. Temperatures increase from top to bottom when $\Delta > -1$.

Appendix D: The XXX model

The XXX model is given by the following Hamiltonian,

$$H = J \sum_{j=1}^L (\sigma_j^x \sigma_{j+1}^x + \sigma_j^y \sigma_{j+1}^y + \sigma_j^z \sigma_{j+1}^z). \quad (D1)$$

This model is essentially the XXZ model with $\Delta = 1$, where we can now change the sign of the whole Hamiltonian by varying the parameter J . As before, we use periodic boundary conditions. The XXX model has one QCP, located at $J = 0$. For $J < 0$ we have the ferromagnetic phase and for $J > 0$ the antiferromagnetic one.

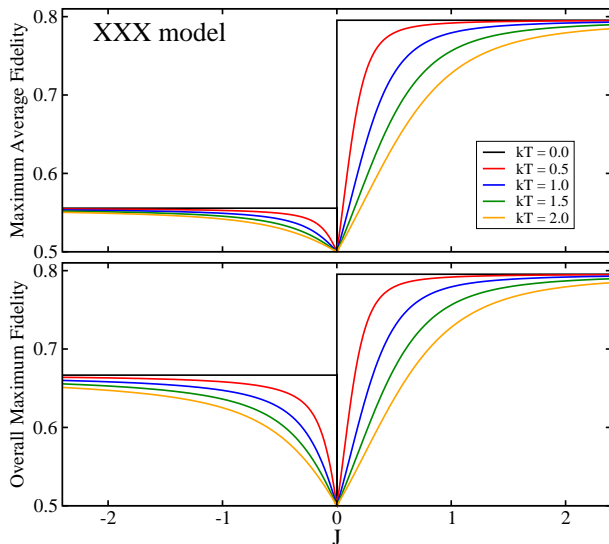


FIG. 14: (color online) $\langle \overline{\mathcal{F}} \rangle$ (upper panel) and $\overline{\mathcal{F}}$ (lower panel) for a spin-1/2 chain in the thermodynamic limit.

In Fig. 14 we show $\langle \overline{\mathcal{F}} \rangle$ and $\overline{\mathcal{F}}$ as a function of J for several values of temperature. It is clear from those figures that both $\langle \overline{\mathcal{F}} \rangle$ and $\overline{\mathcal{F}}$ detect the QCP at finite T , similar to what one obtains computing the thermal quantum discord [11]. Also, for $kT \gtrsim 0.1$ the entanglement is already zero before, at, and after the QCP [11].

-
- [1] S. Sachdev, Quantum Phase Transitions (Cambridge University Press, Cambridge, 1999).
- [2] M. Greiner, O. Mandel, T. Esslinger, T. W. Hänsch, and I. Bloch, Nature (London) **415**, 39 (2002).
- [3] V. F. Gantmakher and V. T. Dolgoplov, Phys. Usp. **53**, 1 (2010).
- [4] S. Rowley, R. Smith, M. Dean, L. Spalek, M. Sutherland, M. Saxena, P. Alireza, C. Ko, C. Liu, E. Pugh *et al.*, Phys. Status Solidi B **247**, 469 (2010).
- [5] L.-A. Wu, M. S. Sarandy, and D. A. Lidar, Phys. Rev. Lett. **93**, 250404 (2004).
- [6] T. R. de Oliveira, G. Rigolin, M. C. de Oliveira, and E. Miranda, Phys. Rev. Lett. **97**, 170401 (2006); T. R. de Oliveira, G. Rigolin, and M. C. de Oliveira, Phys. Rev. A **73**, 010305 (2006); T. R. de Oliveira, G. Rigolin, M. C. de Oliveira, and E. Miranda, Phys. Rev. A **77**, 032325(R) (2008).
- [7] R. Dillenschneider, Phys. Rev. B **78**, 224413 (2008).
- [8] M. S. Sarandy, Phys. Rev. A **80**, 022108 (2009).
- [9] W. K. Wootters, Phys. Rev. Lett. **80**, 2245 (1998).
- [10] T. Werlang and G. Rigolin, Phys. Rev. A **81**, 044101 (2010).
- [11] T. Werlang, C. Trippe, G. A. P. Ribeiro, G. Rigolin, Phys. Rev. Lett. **105**, 095702 (2010); T. Werlang, G. A. P. Ribeiro, and G. Rigolin, Phys. Rev. A **83**, 062334 (2011); T. Werlang, G. A. P. Ribeiro, and G. Rigolin, Int. J. Mod. Phys. B **27**, 1345032 (2013).
- [12] TQD is the QD computed for systems in equilibrium with a thermal reservoir at temperature T .
- [13] H. Ollivier and W. H. Zurek, Phys. Rev. Lett. **88**, 017901 (2001).
- [14] L. Henderson and V. Vedral, J. Phys. A: Math. Gen. **34**, 6899 (2001).
- [15] Y. Huang, New J. Phys. **16**, 033027 (2014).
- [16] A. L. Malvezzi, G. Karpat, B. Çakmak, F. F. Fanchini, T. Debarba, and R. O. Vianna, Phys. Rev. B **93**, 184428 (2016).
- [17] C. H. Bennett, G. Brassard, C. Crepeau, R. Jozsa, A. Peres, and W. K. Wootters, Phys. Rev. Lett. **70**, 1895 (1993).
- [18] Y. Yeo, e-print arXiv:quant-ph/0205014; Y. Yeo, Phys. Rev. A **66**, 062312 (2002).
- [19] R. Fortes and G. Rigolin, Phys. Rev. A **96**, 022315 (2017).
- [20] M. Takahashi, Thermodynamics of one-dimensional solvable models (Cambridge University Press, Cambridge, 1999).
- [21] A. Klümper, Ann. Phys. **1**, 540 (1992); Z. Phys. B **91**, 507 (1993).
- [22] M. Bortz and F. Göhmann, Eur. Phys. J. B **46**, 399 (2005).
- [23] H. E. Boos, J. Damerau, F. Göhmann, A. Klümper, J. Suzuki, and A. Weiße, J. Stat. Mech. (2008) P08010.
- [24] C. Trippe, F. Göhmann, and A. Klümper, Eur. Phys. J. B **73**, 253 (2010).
- [25] A. Uhlmann, Rep. Math. Phys. **9**, 273 (1976).
- [26] R. Fortes and G. Rigolin, Phys. Rev. A **92**, 012338 (2015); Z. J. **93**, 062330 (2016).
- [27] G. Gordon and G. Rigolin, Phys. Rev. A **73**, 042309 (2006); **73**, 062316 (2006); Eur. Phys. J. D **45**, 347 (2007).
- [28] When we refer to Eq. (12) we use the term “mean fidelity” while we reserve the term “average fidelity” for Eq. (13).
- [29] X. Rong, J. Geng, F. Shi, Y. Liu, K. Xu, W. Ma, F. Kong, Z. Jiang, Y. Wu, and J. Du, Nat. Commun. **6**, 8748 (2015).
- [30] C. E. Bradley, J. Randall, M. H. Abobeih, R. C. Berrevoets, M. J. Degen, M. A. Bakker, M. Markham, D. J. Twitchen, and T. H. Taminiau, Phys. Rev. X **9**, 031045 (2019).
- [31] T. Xie, Z. Zhao, X. Kong, W. Ma, M. Wang, X. Ye, P. Yu, Z. Yang, S. Xu, P. Wang *et al.*, Sci. Adv. **7**, eabg9204 (2021).
- [32] A. Noiri, K. Takeda, T. Nakajima, T. Kobayashi, A. Sam-

- mak, G. Scappucci, and S. Tarucha, *Nature* **601**, 338 (2022).
- [33] X. Xue, M. Russ, N. Samkharadze, B. Undseth, A. Sammak, G. Scappucci, and L. M. Vandersypen, *Nature* **601**, 343 (2022).
- [34] M. T. Mađzik, S. Asaad, A. Youssry, B. Joecker, K. M. Rudinger, E. Nielsen, K. C. Young, T. J. Proctor, A. D. Baczewski, A. Laucht *et al.*, *Nature* **601**, 348 (2022).
- [35] T. Xie, Z. Zhao, S. Xu, X. Kong, Z. Yang, M. Wang, Y. Wang, F. Shi, and J. Du, e-print arXiv:2212.02831 [quant-ph].
- [36] P. N. Timonin, *J. Exp. Theor. Phys.* **113**, 251 (2011).
- [37] O. Rojas, J. Strečka, O. Derzhko, and S. M. de Souza, *J. Phys.: Condens. Matter* **32**, 035804 (2020).
- [38] M. A. Nielsen and I. L. Chuang, *Quantum Computation and Quantum Information* (Cambridge University Press, Cambridge, 2000).
- [39] We have N complex coefficients leading to $2N$ real parameters. However, since an overall phase is irrelevant and we must satisfy the normalization constraint, we are left with $2N - 2$ independent parameters.